Origin of large dark current increase in InGaAs/InP avalanche photodiode

J. Wen,[1,2] W. J. Wang,[1,a)] X. R. Chen,[1] N. Li,[1] X. S. Chen,[1] and W. Lu[1,a)]
[1]*State Key Laboratory of Infrared Physics, Shanghai Institute of Technical Physics, Chinese Academy of Sciences, Shanghai 200083, China*
[2]*University of Chinese Academy of Sciences, Beijing 100000, China*

(Received 9 August 2017; accepted 28 October 2017; published online 17 November 2017)

The large dark current increase near the breakdown voltage of an InGaAs/InP avalanche photodiode is observed and analyzed from the aspect of bulk defects in the device materials. The trap level information is extracted from the temperature-dependent electrical characteristics of the device and the low temperature photoluminescence spectrum of the materials. Simulation results with the extracted trap level taken into consideration show that the trap is in the InP multiplication layer and the trap assisted tunneling current induced by the trap is the main cause of the large dark current increase with the bias from the punch-through voltage to 95% breakdown voltage. *Published by AIP Publishing*. https://doi.org/10.1063/1.4999646

I. INTRODUCTION

Geiger mode InGaAs/InP avalanche photodiode infrared detectors (APDs) are widely used in many applications such as quantum communication,[1–4] photon counting,[5] laser ranging,[6] laser radar imaging,[7,8] and high-resolution biochemistry detection.[9] For APDs, Geiger working mode is when the devices work under the reverse bias voltage (V_{bias}) above the breakdown voltage (V_b). Therefore, due to the high multiplication factor under Geiger mode, the multiplied bulk dark current is dominant, which is closely related to the quality of the materials and the fabrication processes.[10,11] So, it is vital to find out the main dark current components due to the traps in the material. Analysis of the dominant dark current components in linear mode could give information about the traps, which would provide guidance for the Geiger mode performance improvement such as the dark count rate and after pulsing characteristics.[12–16]

In this paper, the dark current increase in linear mode of devices with different diffusion temperatures is analyzed. The trap level in the material is extracted from the low temperature photoluminescence (PL) spectrum and temperature dependent $I \sim V$ measurements. The extracted trap level is introduced into the theoretical simulation, and the main dark current component is obtained.

II. STRUCTURE AND EXPERIMENTAL RESULTS

The devices analyzed in the paper were fabricated with the structure of planer separate absorption, grading, charge, and multiplication (SAGCM), denoted in Fig. 1(a). Two zinc diffusion processes were made in the InP cap layer to form the guard ring structure and a 0.3 μm InP multiplication layer. Surface charge density of the InP charge layer is to $2.4 \times 10^{12}\,\mathrm{cm}^{-2}$. The undoped $In_{0.53}Ga_{0.47}As$ absorption layer is 1.5 μm thick. Two types of devices (denoted as device A and device B) with different diffusion processes are presented in the paper for comparison and analysis. The diffusion temperatures for device A and device B are 485 °C and 515 °C, respectively, and the diffusion time is modified to maintain the same diffusion depth.

Figure 1(b) shows the dark current characteristics of device A and device B. We can see that dark current of device A increases from 1×10^{-10} A to 1×10^{-8} A when V_{bias} increases from 15 V to 42 V, covering the range from the punch-through voltage (V_p) to 95% breakdown voltage V_b. An increase of two orders of magnitude is found in device A. While in device B, the dark current increases from 1.5×10^{-10} A to 1.5×10^{-9} A when V_{bias} changes from V_p to 95% V_b, showing only one order of magnitude, which is similar to other reports.[17,18] The large dark current increase in device A indicates the existence of large bulk dark current. Since the bulk dark current is closely related to the material defects, it is very important to find out the main source of the dark current and obtain the trap level information.

The temperature dependent $I \sim V$ characteristics of device A and device B are shown in Fig. 2. The $I \sim V$ curves under different temperatures reflect the variation of dominant current components, which can be quantitatively expressed by the activation energy E_a.[19,20] $\ln I$ is in linear relationship with $1/T$ according to the definition of $I = A\exp(-E_a/k_BT)$. If the slope of $\ln I \sim 1000/T$ is set as K, E_a can be expressed as $E_a = -K \cdot 10^3 k_B \cdot \ln 10$, where I is the total dark current, k_B is the Boltzmann constant, T is the temperature. Based on the results in Fig. 2, linear fit of $\ln I \sim 1000/T$ curves under different V_{bias} are conducted in Figs. 3(a) and 3(b). The corresponding values of activation energy for device A and device B are listed in Table I.

Figure 3(c) shows the $E_a \sim V_{bias}$ diagrams for device A and B. E_a indicates the dark current generation mechanisms of the device, which combines the effect of material bandgap and trap level. The main trap-related components of bulk dark current include generation-recombination (GR) current and trap assisted tunneling (TAT) current.

The GR and TAT dark current components are defined as follows, respectively:

$$I_{GR} = (qn_iAw/\tau_{eff})[1 - \exp(-qV_{bias}/2k_BT)], \quad (1)$$

a)Authors to whom correspondence should be addressed: wangwj@mail.sitp.ac.cn and luwei@mail.sitp.ac.cn

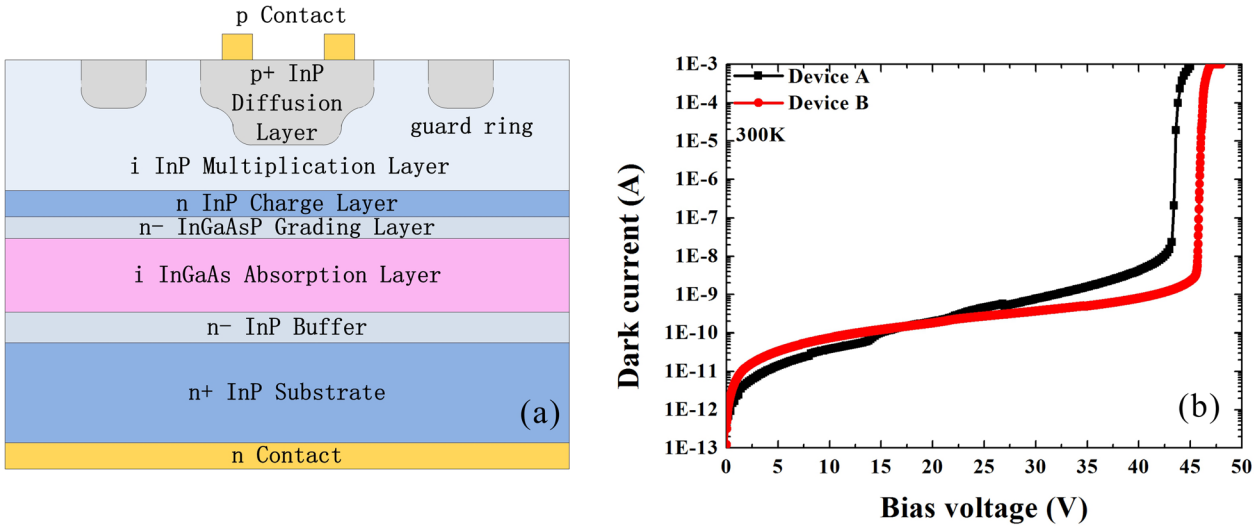

FIG. 1. (a) Material structure of devices. (b) Dark current of device A and device B.

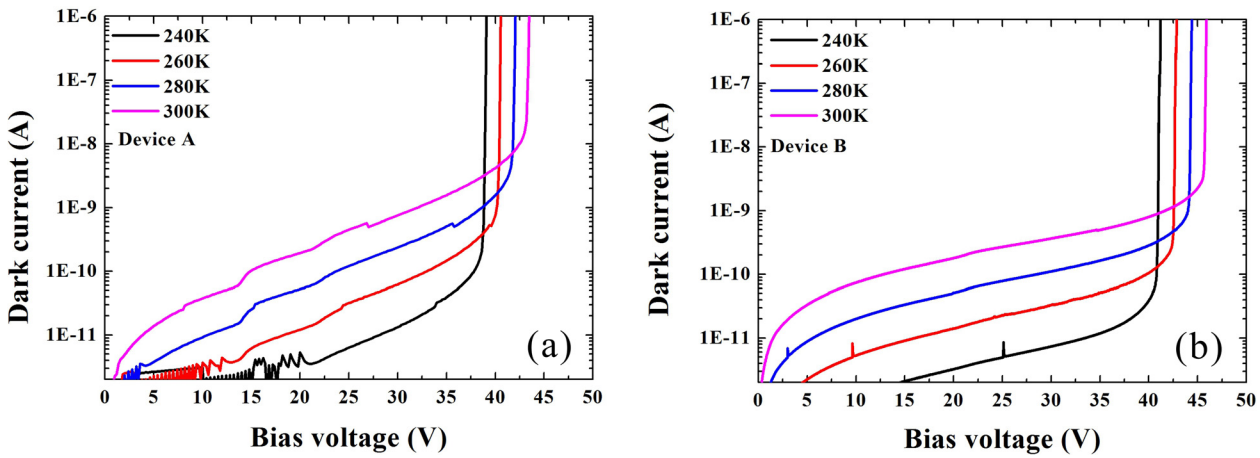

FIG. 2. $I \sim V$ characteristics measured under different temperatures.

TABLE I. Activation energies of different bias voltages for device A and device B.

V_{bias} (V)		15	17	19	21	23	25	27	29	31	33	35
E_a (eV)	A	0.4746	0.4733	0.4687	0.4568	0.4610	0.4409	0.4277	0.4247	0.4144	0.3994	0.3804
	B	0.4344	0.4302	0.4275	0.4275	0.4246	0.4159	0.4150	0.4081	0.4035	0.3971	0.3817

$$I_{TAT} = CE_m V_{bias} A \exp\left(-\theta m_0^{1/2} \varepsilon_g^{3/2} / q\hbar E_m\right). \quad (2)$$

Here, q is the elementary charge, n_i is the intrinsic carrier concentration, A is the device area, w is the length of the depletion region, τ_{eff} is the minority carrier life time, V_{bias} is the bias voltage, k_B is the Boltzmann constant, T is the temperature, E_m is the maximum electric field, ε_g is the bandgap, m_0 is the electron effective mass, and C and θ are the constants depending on the material traps and tunneling barrier shape.

Considering the relationship of I_{GR} and I_{TAT} with T, I_{GR} can be easily decreased by reducing the working temperature, while I_{TAT} remains almost the same with the changing temperature. The relationship of I_{GR} and I_{TAT} with V_{bias} shows that I_{TAT} is proportional to the square of V_{bias}, while I_{GR} varies little with V_{bias} above the value of several k_BT/q. The decrease of E_a means the lower temperature dependence and lower threshold barrier for dark current with the increasing V_{bias}, which indirectly indicates I_{TAT} to be the main cause of the large dark current increase near V_b. This is also confirmed in other reports using empirical formula fitting to do the dark current analysis.[18] From Fig. 3(c), we can see that in device B, the slope of $E_a \sim V_{bias}$ is smaller, which indicates that the percentage of TAT current in the total dark current in device B is less than that in device A.

The low temperature photoluminescence spectrum measurements were made on the materials of device A and B with the corresponding same diffusion processes. In order to avoid the influence of dopants to the PL test, no Zinc is added in the diffusion process. As shown in Fig. 4, a trap level, which is 0.468 eV away from the valence band is

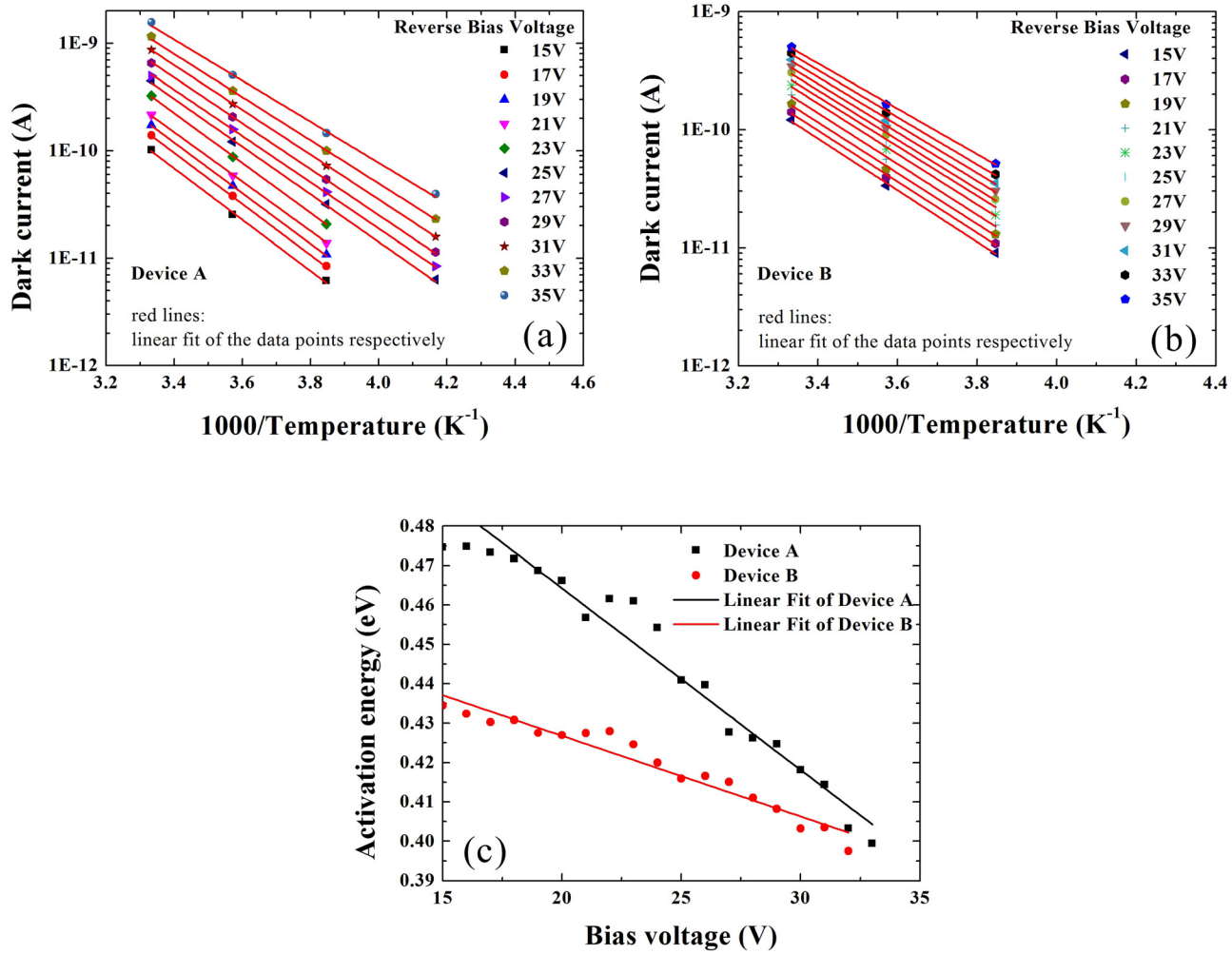

FIG. 3. (a) Linear fit of $\ln I \sim 1000/T$ under different reverse bias voltages for device A. (b) Linear fit of $\ln I \sim 1000/T$ under different reverse bias voltages for device B. (c) Scattered dots diagrams and their linear fit of $E_a \sim V_{bias}$ for device A and B.

found in the material with the same diffusion temperature (485 °C) as device A, which corresponds with the extracted E_a. No such trap is found in the material with 515 °C diffusion process as device B. All the samples for PL spectrum measurements are prepared with no zinc presented during the diffusion process, so the difference in PL spectra is caused by the temperature rather than the dopant.

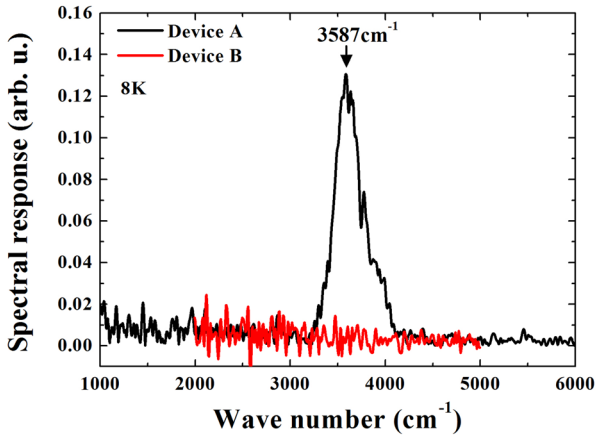

FIG. 4. PL spectra of device A and device B measured under the temperature of 8 K.

From the above experimental results, we obtained the changing trends of the main dark current components with the increasing bias voltages and found the existence of a trap level in the lower temperature diffused material. But the origin of the trap and how the trap affects the dark current remain unknown. Therefore, further theoretical analysis with the trap level taken into consideration is as follows.

III. NUMERICAL METHOD AND WORKING MECHANISM

The following current components are taken into consideration in the simulation: diffusion current I_{diff}, thermal generation-recombination current I_{GR}, trap assisted tunneling current I_{TAT}, direct radiative combination current $I_{Radiative}$, Auger recombination current I_{Auger}, band-to-band tunneling current I_{B2B}. Simulations are conducted using Sentaurus Workbench with drift-diffusion model as the basic model. The physical structural model of the device is built along the material growth direction. The effect of guard ring is neglected in this model for simplification because we emphasize on the bulk leakage current. $I \sim V$ characteristics are obtained by solving the Poisson equation coupled with the carrier continuity equation. The simulations lay emphasis on

the effect of traps in the material. Thermal GR current can be expressed using Shockley-Read-Hall (SRH) model in Sentaurus when SRH model is activated with only doping and temperature dependent parameters. TAT current model is integrated in the SRH, so thermal GR current component is obtained by subtracting TAT current from the total SRH current when TAT component is taken into consideration.[21,22] TAT current is modified from the SRH current by introducing field enhancement factor Γ_n (for electrons) and Γ_p (for holes) to show the effect of the strong electric field on carrier lifetime. Therefore, the recombination rate by TAT and SRH mechanisms are defined as follows:

$$R_{TAT} = \frac{pn - n_i^2}{\frac{\tau_p}{1+\Gamma_p}\left[n + n_i \exp\left(\frac{E_{trap} - E_i}{k_B T}\right)\right] + \frac{\tau_n}{1+\Gamma_n}\left[p + n_i \exp\left(\frac{E_i - E_{trap}}{k_B T}\right)\right]}, \tag{3}$$

$$R_{SRH} = \frac{pn - n_i^2}{\tau_p\left[n + n_i \exp\left(\frac{E_{trap} - E_i}{k_B T}\right)\right] + \tau_n\left[p + n_i \exp\left(\frac{E_i - E_{trap}}{k_B T}\right)\right]}, \tag{4}$$

where n, p, and n_i are the electron, hole, and the intrinsic carrier concentration, respectively; E_{trap} is the trap level; E_i is the intrinsic level; k_B is the Boltzmann constant; and T is the temperature. Trap level parameters are extracted from the PL spectrum measurement.

IV. RESULTS AND DISCUSSION

Figure 5 shows the simulated dark current components. In Fig. 5(a) the measured trap level is set in the InP multiplication layer. The trap level is set to −0.207 eV (0.468–1.35/2 = −0.207 eV) relative to the mid-bandgap with the trap level located at 0.468 eV above the valance band according to the PL spectrum measurement. Carrier life time is set as 10 μs according to the empirical values.[10,22,23] As shown in Fig. 5(a), the total current originated from the traps in the InP multiplication layer increases from 4.57×10^{-12} A to 4.39×10^{-10} A when V_{bias} changes from V_p to 95% V_b, with two orders of magnitude. The TAT current I_{TAT} is greater than the thermal GR current I_{GR}, becoming the dominant component of the dark current induced by the traps in the InP multiplication layer.

In Fig. 5(b), the measured trap level is set in the InGaAs absorption layer. The trap level is set to 0.093 eV (0.468–0.75/2 = 0.093 eV) relative to the mid-bandgap of $In_{0.53}Ga_{0.47}As$. The total current increases from 1.45×10^{-11} A to 1.85×10^{-10} A when V_{bias} changes from V_p to 95%V_b, with only one order of magnitude. I_{GR} is definitely the dominant component while the second leading component I_{TAT} is one order less than I_{GR}.

Combining the simulation results with the extracted E_a and PL spectra, the trap level measured by PL in device A is in the InP multiplication layer, and the TAT current is the dominant dark current near V_b, which is contributed to the increase of two orders of magnitude of dark current. Other reports[14] also revealed that TAT current in the InP multiplication layer is dominant at high trap concentration, while the trap level adopted in these simulations was empirical value. The trap level extracted from the PL spectrum measurement in our work can help provide an exact value for the dark current simulation. Since APD usually works under the temperature of about 220 K, I_{GR} could be suppressed by the low temperature. It is necessary to suppress I_{TAT} to obtain lower dark current near V_b. Therefore, the optimized

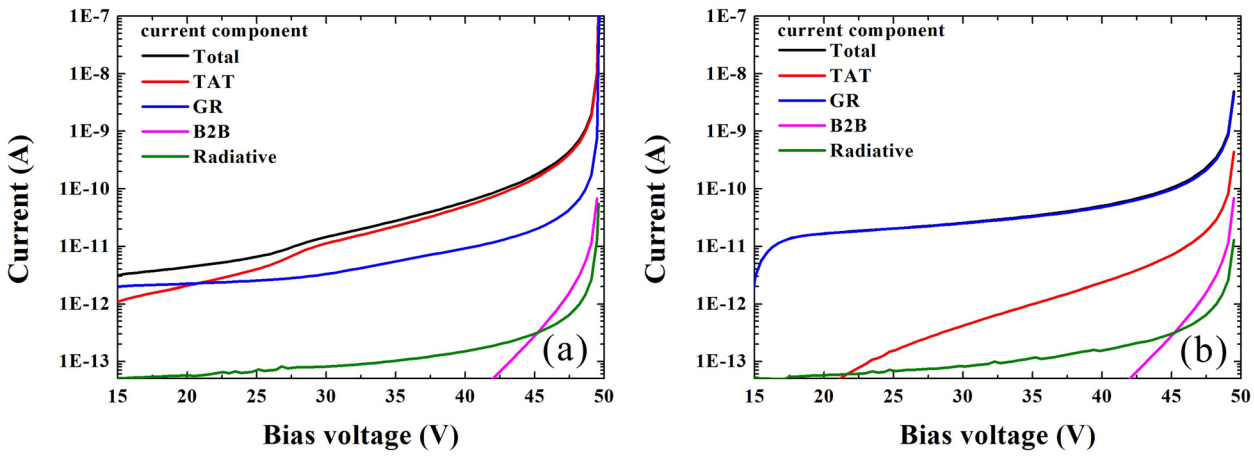

FIG. 5. (a) Current components extracted from the simulated dark current with the trap level of −0.207 eV in the InP multiplication layer taken into consideration. (b) Current components extracted from the simulated dark current with the trap level of 0.093 eV in the InGaAs absorption layer taken into consideration.

diffusion temperature is 515 °C as applied on device B. Further tests on the two devices in Geiger mode show that the dark count rate of device B is one order less than that of device A under the same test condition, which provides a way to improve the performance of an InGaAs/InP APD.

V. CONCLUSIONS

Two types of APD devices with different temperature diffusion processes were fabricated. Temperature dependent $I \sim V$ characteristics of the two devices were measured and the activation energies under different bias voltages were extracted. The decrease of E_a with the increasing V_{bias} indicates the TAT current to be the main cause of the large dark current increase near the breakdown voltage. And the percentage of TAT current in the total dark current in the higher temperature diffused device is less than that in the lower temperature diffused one. A trap level, which is 0.468 eV above the valence band, is found through the low temperature PL measurement in the lower temperature diffused material. Simulation results show that the trap is located in the InP multiplication layer and the corresponding TAT current is the dominant dark current near V_b, which contributes to the increase of two orders of magnitude of dark current.

ACKNOWLEDGMENTS

This work was supported by National Key R&D Program of China (2016YFB0402404), Natural Science Foundation of China (61405231), Shanghai Science and Technology Foundation (16JC1400404), and Key research project of Frontier Science of Chinese Academy of Sciences (QYZDJ-SSW-JSC007).

[1]X. Jiang, M. A. Itzler, K. O'Donnell, M. Entwistle, M. Owens, K. Slomkowski, and S. Rangwala, IEEE J. Sel. Top. Quantum Electron. **21**, 3800112 (2015).
[2]D. F. V. James, Phys. Today **54**(11), 60 (2001).
[3]R. H. Hadfield, Nat. Photonics **3**, 696 (2009).
[4]C. Z. Peng, J. Zhang, D. Yang, W. B. Gao, H. X. Ma, H. Yin, H. P. Zeng, T. Yang, X. B. Wang, and J. W. Pan, Phys. Rev. Lett. **98**, 010505 (2007).
[5]P. A. Hiskett, G. S. Buller, A. Y. Loudon, J. M. Smith, I. Gontijo, A. C. Walker, P. D. Townsend, and M. J. Robertson, Appl. Opt. **39**, 6818 (2000).
[6]A. McCarthy, X. Ren, A. D. Frera, N. R. Gemmell, N. J. Krichel, C. Scarcella, A. Ruggeri, A. Tosi, and G. S. Buller, Opt. Express **21**, 22098 (2013).
[7]M. A. Itzler, U. Krishnamachari, M. Entwistle, X. Jiang, M. Owens, and K. Slomkowski, IEEE J. Sel. Top. Quantum Electron. **20**, 3802111 (2014).
[8]M. A. Albota, R. M. Heinrichs, D. G. Kocher, D. G. Fouche, B. E. Player, M. E. O'Brien, B. F. Aull, J. J. Zayhowski, J. Mooney, B. C. Willard, and R. R. Carlson, Appl. Opt. **41**, 7671 (2002).
[9]L. Zhu, W. J. Stryjewski, and S. A. Soper, Anal. Biochem. **330**, 206 (2004).
[10]F. Acerbi, M. Anti, and A. Tosi, IEEE Photonics J. **5**, 6800209 (2013).
[11]S. Pellegrini, R. E. Warburton, L. J. J. Tan, J. S. Ng, A. B. Krysa, K. Groom, J. P. R. David, S. Cova, M. J. Robertson, and G. S. Buller, IEEE J. Quantum Electron. **42**, 397 (2006).
[12]B. Korzh, T. Lunghi, K. Kuzmenko, G. Boso, and H. Zbinden, J. Mod. Opt. **62**, 1151 (2015).
[13]F. X. Wang, W. Chen, Y. P. Li, D. He, C. Wang, Y. G. Han, S. Wang, Z. Q. Yin, and Z. F. Han, J. Lightwave Technol. **34**, 3610 (2016).
[14]J. Xu, X. S. Chen, W. J. Wang, and W. Lu, Infrared Phys. Technol. **76**, 468 (2016).
[15]M. A. Itzler, X. Jiang, M. Entwistle, K. Slomkowski, A. Tosi, F. Acerbi, F. Zappa, and S. Cova, J. Mod. Opt. **58**, 174 (2011).
[16]J. Zhang, M. A. Itzler, H. Zbinden, and J. W. Pan, Light: Sci. Appl. **4**, e286 (2015).
[17]F. Acerbi, A. Tosi, and F. Zappa, Sens. Actuators, A **201**, 207 (2013).
[18]Y. L. Zhao, D. D. Zhang, L. Qin, Q. Tang, R. H. Wu, J. J. Liu, Y. P. Zhang, H. Zhang, X. H. Yuan, and W. Liu, Opt. Express **19**, 8546 (2011).
[19]G. Cao, T. Li, H. Tang, X. Shao, X. Li, and H. Gong, Proc. SPIE **9284**, 928406 (2014).
[20]S. Bothra, S. Tyagi, S. K. Ghandhi, and J. M. Borrego, Solid-State Electron. **34**, 47 (1991).
[21]X. Ji, B. Liu, Y. Xu, H. Tang, X. Li, H. Gong, B. Shen, X. Yang, P. Han, and F. Yan, J. Appl. Phys. **114**, 224502 (2013).
[22]Q. Y. Zeng, W. J. Wang, J. Wen, P. X. Xu, W. D. Hu, Q. Li, N. Li, and W. Lu, Opt. Quantum Electron. **47**, 1671 (2015).
[23]Q. Y. Zeng, W. J. Wang, J. Wen, L. Huang, X. H. Liu, N. Li, and W. Lu, J. Appl. Phys. **115**, 164512 (2014).